Journal of
Water & Climate Change

IWA PUBLISHING

Journal of Water and Climate Change Vol 15 No 2, 518 doi: 10.2166/wcc.2024.448

Characteristics and distribution model of wind and wave in Shengsi mussel culture area under the impacts of tropical cyclones

Zuli Wu, Minsi Xiong, Yongchuang Shi, Yunpeng Song, Yang Dai and Shengmao Zhang*

Key Laboratory of Fisheries Resources Remote Sensing and Information Technology Resources, East China Sea Fisheries Research Institute, Chinese Academy of Fisheries Science, Shanghai 200090, China
*Corresponding author. E-mail: zhangsm@ecsf.ac.cn

ZW, 0009-0006-9395-1658

ABSTRACT

The primary industry in Shengsi County, Zhejiang Province, China, is the raft-based cultivation of *Mytilus coruscus*, which is highly sensitive to wind and wave disturbances. This study aims to understand the characteristics of tropical cyclones along Zhejiang's coast, their relation to climate change, and the impact of wind and waves on Shengsi mussel farming during cyclones. Analyzing data from 2000 to 2018, including tropical cyclone paths, wind and wave data, and mussel farming statistics, the research identifies four cyclone path types, with the peak prevalence from July to September. Annual cyclone energy fluctuates, peaking in August. In the cyclone impact zone, the average wind speed is 24.59 m/s. Type D cyclones have the most significant impact. A linear relationship exists between cyclone center distance and wind speed/wave height. Extreme wind speed and wave height follow the Gumbel joint probability distribution. Since 2000, the Shengsi mussel farming area experienced an 11.20-year return period for wind and waves from the strongest cyclone, Muifa. Given the recurrence period of Muifa intensity cyclones in 2020 and the following years, the study recommends disaster preparedness for the Shengsi mussel farming area and emphasizes the role of mutual aid insurance.

Key words: typhoon, fisheries mutual aid insurance, floating raft aquaculture, wind and wave model

HIGHLIGHT

- This paper's innovative approach, development of a localized model, practical implications for adaptation and disaster management, and contribution to coastal science collectively enhance our understanding of the complex interplay between water, climate change, and aquaculture in the face of tropical cyclones.

GRAPHICAL ABSTRACT

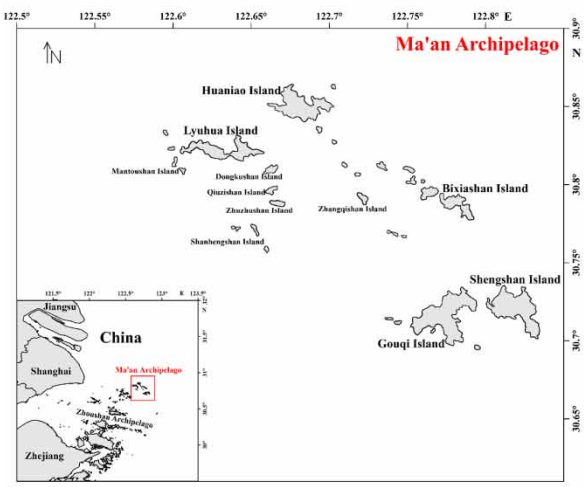

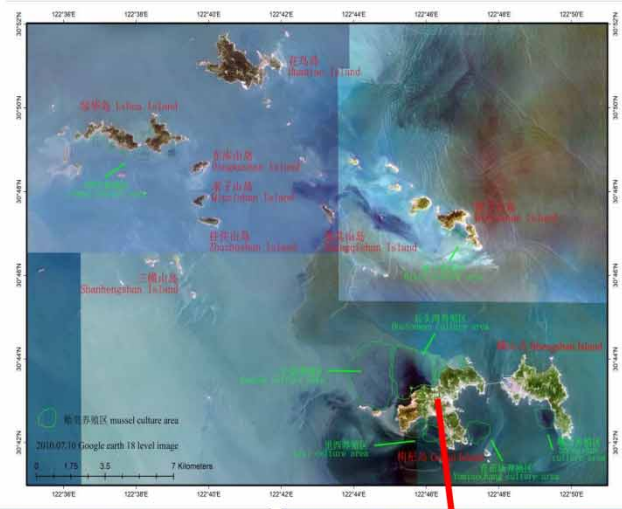

Shengsi mussel Aquaculture Industry:

- Cultivation Area: 1,450 hectares
- Production: 206,400 tons (approximately 13.69% of the world's mussel production)
- Number of Cultivators: 1,100 households
- Workforce: Over 6,000 people
- Output Value: 770 million yuan

Research Background: The Impact of Super Typhoon "Muifa" in 2011 on the Shengsi Mussel Aquaculture Industry

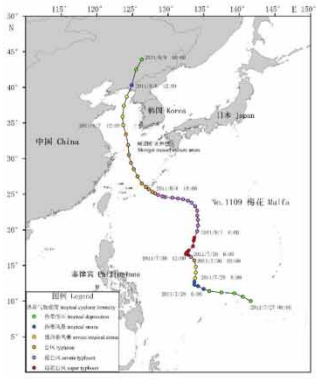

The path of Super Typhoon Muifa

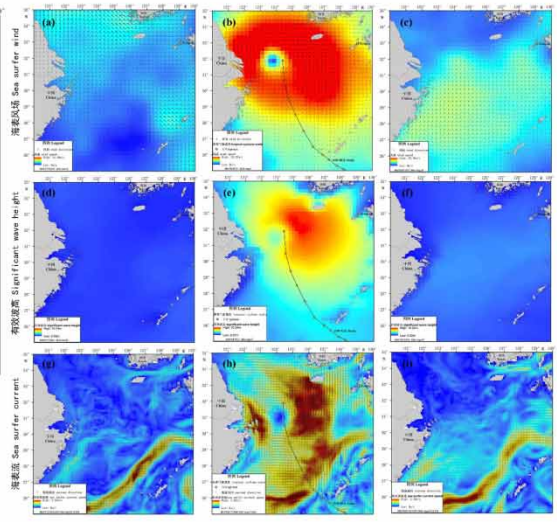

The disturbance of Super Typhoon Muifa on the marine environment

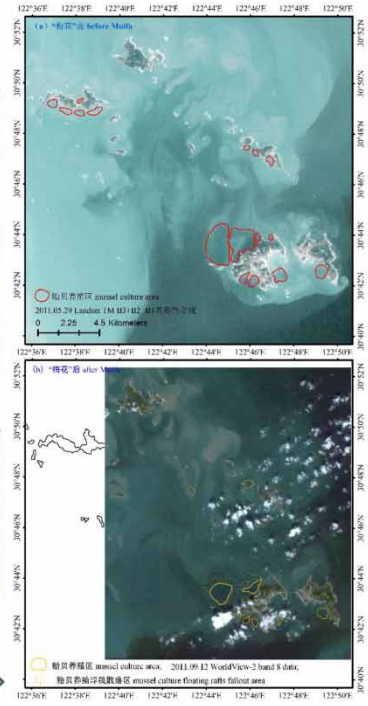

Distribution changes in the Shengsi mussel farming area before and after the impact of Super Typhoon Muifa

Research Background: The Impact of Severe Typhoon “Talim" in 2017 on the Shengsi Mussel Aquaculture Industry

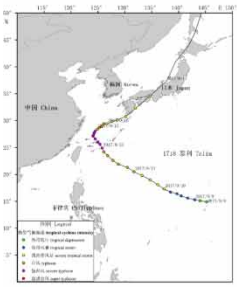

The path of Talim

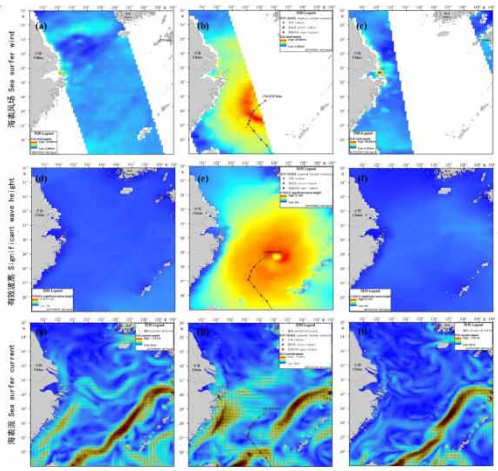

The disturbance of Talim on the marine environment

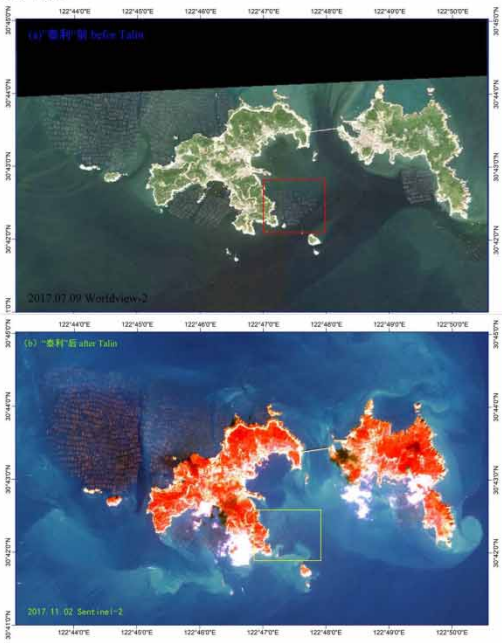

Distribution changes in the Shengsi mussel farming area before and after the impact of Talim

Research Content:

1.Characteristics of tropical cyclones along the Zhejiang coast and their relationship with climate change.
2.The response of wind and waves in the Shengsi mussel farming area to tropical cyclone activity.
3.Construction of a joint distribution model for wind and waves in the Shengsi mussel farming area.
4.Setting wind and wave conditions for Shengsi mussel farming insurance and providing disaster prevention and mitigation recommendations.

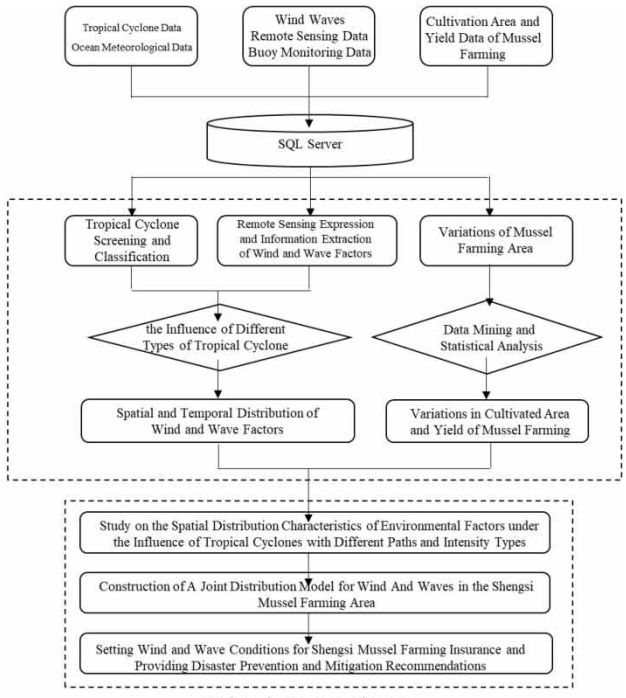

Technology Roadmap

The family Mytilidae exhibit a wide distribution ranging from temperate to polar, and subtropical to tropical marine zones. Renowned for their robust growth density and strong attachment capabilities, mussels are well recognized for their unique physiological abilities, primarily attributed to their adhesive organ known as 'byssus threads.' Initially described by Brown, the byssus threads in bivalves are extracellular collagen structures secreted by the foot, comprising a proximal end, a distal end, and adhesive plaques (Brown 1952). Mussels utilize byssus threads for attachment in intertidal zones or aquaculture hanging rope substrates, and they can even attach to other mussel individuals, forming aggregations that eventually create large cohesive structures known as 'mussel beds'.

China's marine aquaculture contributes to a total bivalve production of 14.80 million tons, representing 70% of marine aquaculture production. The cultivation area spans 1.1974 million ha, covering over 60% of China's marine aquaculture area (China Ministry of Agriculture and Rural Affairs, Bureau of Fisheries and Fisheries Law Enforcement 2021). The bivalve aquaculture industry serves as a crucial pillar in China's aquaculture economy, with shallow-water raft culture being a predominant mode (Wang & Zheng 2004; Lin *et al.* 2016). Mussels, being significant species in the aquaculture sector, are extensively cultivated globally, notably in regions such as Northern Europe, North America, Australia, and China, resulting in substantial production and yields (Seuront *et al.* 2019; Roberts *et al.* 2021; Wu *et al.* 2021).

Mytilus coruscus belonging to the Mytilidae family is primarily distributed in the northwest Pacific, including Japan's Hokkaido, South Korea's Jeju Island, and various regions in China such as the Yellow Sea, Bohai Sea, East China Sea, and Taiwan (Chinese Animal Taxonomy 1997). Artificial cultivation of *M. coruscus* is concentrated in the marine areas of Ma'an Archipelago, Shengsi County, Zhejiang Province, China. The waters in this region are clear and fertile, with strong tidal currents, making raft culture of thick-shelled mussels a leading industry in China (Figure 1). The historical cultivation area for Shengsi's *M. coruscus* reached a peak of 1,645 ha. In 2020, the cultivation area was 1,460 ha, yielding 209,500 tons with a production value of 770 million RMB. The industry involved 1,100 households and over 6,000 workers (Zhoushan Statistics Bureau 2021).

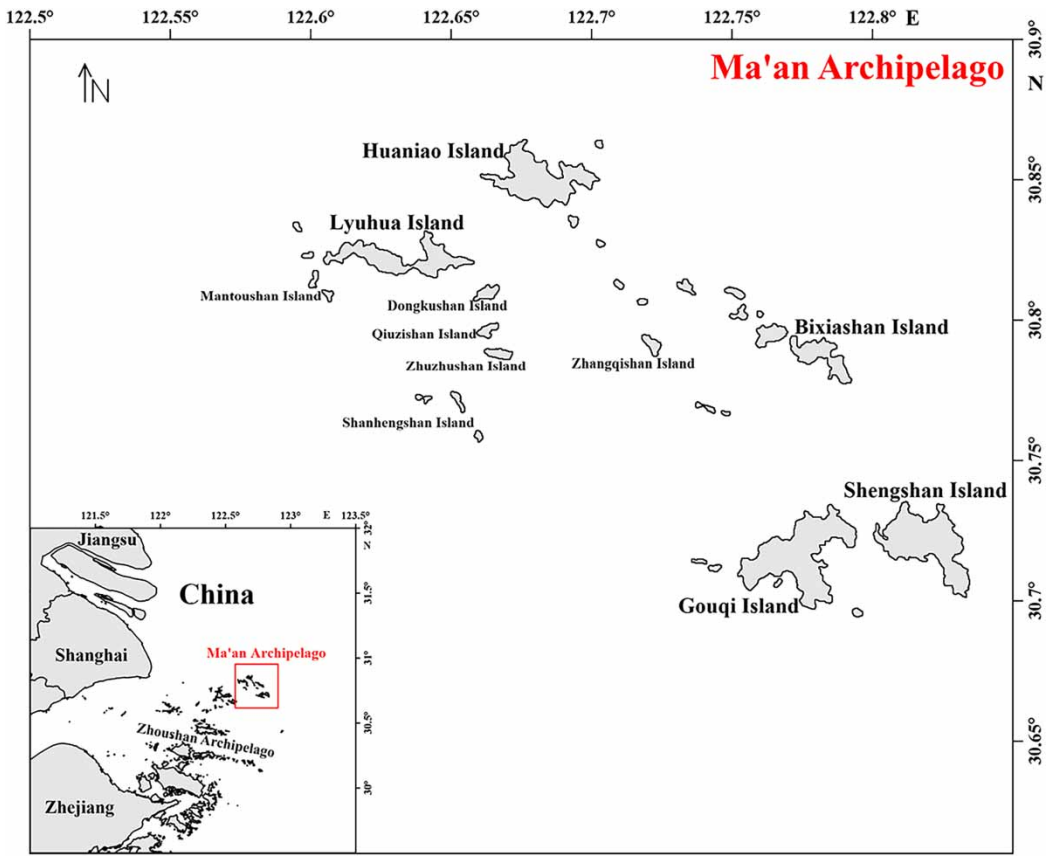

Figure 1 | Distribution of investigative station in Ma'an Archipelago Shengsi County, Zhejiang Province, China.

Raft-cultured mussels exhibit a high tolerance to environmental fluctuations in factors such as temperature, salinity, pH, and wind and wave patterns (Kong *et al.* 2019; Seuront *et al.* 2019; Chao *et al.* 2020; Moyen *et al.* 2020; Jahnsen-Guzmán *et al.* 2022). Ma'an Archipelago in Shengsi County, situated in Zhejiang Province, is the northernmost island town in the Zhoushan Archipelago, outside the Yangtze River estuary. The average annual wind speed in this region is 7.2 m/s, with a maximum wind speed reaching 46.0 m/s, predominantly from south-southeast. The measured maximum tidal current speed is 0.50 m/s, averaging around 0.25 m/s. The average wave height is 1.1 m, with a recorded maximum wave height of 17.0 m. Wind waves of levels 7–9 are concentrated mainly from June to September (China Island, Gazetteer Compilation Committee 2014). It is during this season that *M. coruscus* enter their maturation period. Significant losses in *M. coruscus* cultivation result from severe storm surges caused by tropical cyclones, such as Typhoon Muifa in 2011, which led to a complete failure of 707 ha of *M. coruscus* cultivation in Ma'an Archipelago, resulting in a direct economic loss of 400 million yuan (Wu *et al.* 2021).

Aquaculture is a high-risk, high-input industry. To mitigate risks, provide economic compensation, ensure production stability, and promote post-disaster recovery in agriculture, aquaculture insurance plays a crucial role. However, due to the high-risk nature and profitability of marine aquaculture, traditional insurance products struggle to meet the risk demands of cultivators. Simultaneously, insurance companies are reluctant to engage due to uncontrollable risks, leaving this potentially lucrative industry lacking scientific and effective risk management and mitigation measures (Zhang *et al.* 2017). While fishery mutual insurance provides some basic coverage for cultivators, marine aquaculture insurance mainly focuses on aquatic organisms and plants, leading to challenges in assessing damage and losses in the event of disasters.

In recent years, regions such as Shandong Province and Liaoning Province in China have initiated pilot projects for meteorological index-based aquaculture insurance (Wang 2014; Ying *et al.* 2014; Pan *et al.* 2017). This model determines compensation based on predefined meteorological indices, effectively mitigating challenges in loss assessment. However, when applying this insurance model to mussel scenarios, a comprehensive study of the biological characteristics of the insured objects is still required. Key issues include selecting appropriate meteorological indices and accurately determining the quantitative relationship between meteorological indices and the extent of damage and losses.

Research indicates that water turbulence induced by wind and waves has a direct impact on the growth of mussels. As wind and waves increase water flow velocity, the feeding efficiency of bivalves may improve, thereby promoting growth. However, excessive waves can cause mechanical damage to mussels, affecting their normal physiological activities. Based on the relationship between environmental factor fluctuations and *M. coruscus* production in the raft-cultured area of Ma'an Archipelago, Shengsi, the authors have identified wind and waves as sensitive environmental factors causing losses in *M. coruscus* cultivation (Wu *et al.* 2021). Considering the aforementioned issues, it is worth exploring whether using wind and waves as meteorological insurance indices is scientifically appropriate in the raft-cultured *M. coruscus* industry. If adopting wave indices is confirmed, further research is needed to scientifically quantify the indices and their relationship with the production of damaged *M. coruscus*.

Therefore, this study utilizes tropical cyclone path data provided by the China Meteorological Administration, wind and wave factor buoy measurements provided by the National Marine Administration and foreign ocean remote sensing monitoring service platforms, combined with Shengsi mussel aquaculture production and area data from the Zhoushan Statistical Yearbook. The study analyzes the characteristics and trends of tropical cyclones affecting the Zhejiang region. Based on this, we integrate and construct a joint probability distribution model of wind and waves in the Shengsi area, aiming to quantify the relationship between wind and wave levels during tropical cyclone disasters and the damage to *M. coruscus* cultivation. The purpose of this research is to provide a scientific basis for environmental monitoring and aquaculture insurance services for Shengsi mussel cultivation.

1. MATERIALS AND METHODS

1.1. Tropical cyclone data and selection criteria

The tropical cyclone data used in this study are the tropical cyclone movement path data for the years 2000–2018 provided by the China Meteorological Administration (Ying *et al.* 2014). According to the statistical records in the 'China Meteorological Disaster Encyclopedia' (Zhejiang Volume), tropical cyclones that have an impact on Zhejiang enter the region within 115°–125°E and 25°–32°N (Xi & Xu 2006). Tropical cyclones that do not enter this region have no impact on Zhejiang. Therefore, in this study, 'tropical cyclones' are defined as those with wind speeds $\geq$17.2 m/s when they enter the impact region. A

tropical cyclone will be selected for analysis if its path remains within the impact region for 6 h or more; otherwise, it will not be considered (Yu *et al.* 2014).

1.2. Mussel aquaculture statistical data

The acquisition of the Shengsi mussel aquaculture area and production data is based on the Zhoushan Statistical Yearbook released by the Zhoushan Statistics Bureau from 2002 to 2018 (http://zstj.zhoushan.gov.cn/col/col1228955843/index.html). Data regarding post-disaster mussel losses caused by Typhoon Muifa are derived from the 2011 Shengsi County National Economic and Social Development Statistical Bulletin (https://tjj.zj.gov.cn/art/2012/2/23/art_1229129205_519758.html) and the 2011 Zhejiang Province Ocean Disaster Bulletin (http://gc.mnr.gov.cn/201806/t20180619_1798015.html). Loss data from Shengsi mussel cultivation due to tropical cyclones such as Haikui, Chanhom, Talim, and Ampil from 2007 to 2018 originates from the Shengsi County National Economic and Social Development Statistical Bulletin (http://data.tjj.zj.gov.cn/page/tjData/tjData.jsp?index=0&orgCode=330922) and the Zhejiang Fisheries Mutual Insurance Association's published fishery disaster compensation information (https://www.zfmi.com/zfmi/list/xxgk.pkgs.zs.html).

1.3. Environmental factor data

The sea-surface observed data were obtained from the Shengshan Buoy Observation Station (122.8°E, 30.8°N) published by the National Marine Data and Information Service Center. The monitored data include parameters such as date, wind direction (°), wind speed (m/s), sea water temperature (°C), air pressure (hPa), significant wave height (m), etc. The data cover the period from 1 January 2000, to 31 December 2018, with a recording time scale of 1 h (Wu *et al.* 2020).

The sea-surface significant wave height and sea-surface wind field data were sourced from the Copernicus Marine Environment Monitoring Service (CMEMS) global model data product at level 4. The significant wave height data have a horizontal resolution of 0.083°, while the wind field data have a horizontal resolution of 0.125°. The data include parameters such as longitude, latitude, date, significant wave height (m), wave direction (°), sea-surface wind speed (m/s), and wind direction (°). The data cover the period from 1 January 2000 to 31 December 2018.

1.4. Data analysis and verification

1.4.1. Extraction and analysis of environmental factor data

Wind field and significant wave height data were parsed and extracted using IDL 8.5 software. Environmental factor data were extracted and imported into Access 2010 software to construct an environmental factor database. Date data were merged and matched with the tropical cyclone data created earlier, and environmental factor data for each type of tropical cyclone were extracted.

Based on the distance between the cyclone center coordinates and the center of the study area, the distribution differences of environmental factors among different distance groups for each type of tropical cyclone were analyzed. Variance analysis was conducted using SPSS 19.0 software, with a significance level of $p < 0.05$. Kriging interpolation was applied to simulate the spatial distribution of environmental factor data for each type of tropical cyclone, and raster maps with uniform pixels and the same projection were generated using ArcGIS 10.6 software (Zhang *et al.* 2006; Liu 2017).

1.4.2. Tropical cyclone intensity analysis

Accumulated cyclone energy (ACE) is a measure of the total energy generated by tropical cyclones over a specific period of time. It is calculated by squaring the maximum wind speeds of tropical cyclones reaching tropical storm or higher levels and summing up the squared wind speeds over all relevant time periods. The formula for calculating ACE, as described in Tang & Sui (2015), is as follows:

$$\mathrm{ACE} = \sum_{j}^{m} \sum_{i}^{n} v_i^2$$

where $j = 1,\ldots,m$ represents the number of observations for tropical cyclones reaching tropical storm or higher levels. $i = 1,\ldots,n$ represents the number of observations where the maximum wind speed at the center of the tropical cyclone reaches 17.2 m/s or higher. V_i^2 denotes the square of the maximum wind speed for the ith observation.

1.4.3. Wind and wave joint probability distribution model

The Gumbel model was employed in this study to analyze the joint probability distribution and return period of maximum wind speed and significant wave height in the Shengsi Marine Ranch area during tropical cyclone events.

The joint distribution function of the Gumbel logic model based on Gumbel marginal distributions is given by (Zhou & Duan 2003):

$$F_{XY}(x,y) = e^{-[(-\ln F(x))^m + (-\ln F(y))^m]^{1/m}} (m \geq 1) \tag{1}$$

where $F(x)$ and $F(y)$ represent the marginal distributions of the random variables X and Y, respectively, with their distribution functions given by:

$$\begin{cases} F_X(x) = e^{[-e^{(-x)}]} \\ F_Y(y) = e^{[-e^{(-y)}]} \end{cases} \tag{2}$$

The parameter m represents the correlation between random variables X and Y. When $m = 1$, it indicates that random variables X and Y are completely independent. As m approaches infinity ($m \to \infty$), it signifies that random variables X and Y are fully correlated. Gumbel & Mustafi (1967) and Johnson & Kotz (1972) propose the estimation expression for this parameter as follows:

$$m = \frac{1}{\sqrt{(1-\rho_{XY})}} (0 \leq \rho_{XY} \leq 1) \tag{3}$$

The symbol ρ_{XY} represents the correlation coefficient between random variables X and Y, and its estimation expression is given by:

$$\rho_{XY} = \frac{E[(X-\mu_x)(Y-\mu_y)]}{\sigma_x \sigma_y} \tag{4}$$

The symbols (μ_x, σ_x) and (μ_y, σ_y) represent the mean and standard deviation of random variables X and Y, respectively.

When $m = 1$, meaning the correlation coefficient $\rho_{XY} = 0$ between random variables X and Y, it indicates that random variables X and Y are completely independent. In this case, their joint probability distribution function becomes the product of their marginal distributions, and their joint distribution function can be simply expressed as:

$$F_{XY}(x,y) = F_X(x) F_Y(y) \tag{5}$$

Let the marginal distributions of random variables X and Y be in the following general form:

$$\begin{cases} F_X(x) = e^{[-e^{(-(x-a_x)/b_x)}]} \\ F_Y(y) = e^{[-e^{(y-a_y)/(b_y)}]} \end{cases} \tag{6}$$

In the equation, (a_x, b_x) and (a_y, b_y), respectively, represent the location and scale parameters of the Gumbel distribution for random variables X and Y. They can be obtained using the method of moments from corresponding sub-samples of marginal random variables.

Substituting Equation (6) into Equation (1) and taking partial derivatives with respect to variables x and y on the left side of Equation (1), the joint probability density function for random variables X and Y is obtained as follows:

$$f_{XY}(x,y) = \frac{F_{XY}(x,y)}{b_x b_y} \left\{ e^{\left[-\frac{m(x-a_x)}{b_x}\right]} + e^{\left[-\frac{m(y-a_y)}{b_y}\right]} \right\}^{((1-2m)/m)} \times \left\{ \left[e^{-\frac{m(x-a_x)}{b_x}} + e^{-\frac{m(y-a_y)}{b_y}} \right]^{1/m} + m - 1 \right\} \times e^{\left[-m\frac{(x-a_x}{b_x} + \frac{y-a_y)}{b_y}\right]} \tag{7}$$

The corresponding joint cumulative distribution function for this joint probability density function is:

$$F_{XY}(x,y) = e^{\left\{-\left[e^{\left(-\frac{m(x-a_x)}{b_x}\right)}+e^{\left(-\frac{m(y-a_y)}{b_y}\right)}\right]^{1/m}\right\}} \tag{8}$$

The joint return period $T_{XY}(x, y)$ corresponding to both random variables X and Y exceeding specific values x and y can be obtained using the following equation:

$$T_{XY} = \frac{1}{1 - F_{XY}(x,y)} \tag{9}$$

In this expression, the bivariate joint probability distribution function $F_{XY}(x,y)$ is defined as $P(X \leq x, Y \leq y)$.

Model data consisted of extreme samples of maximum wind speed and corresponding significant wave height recorded at buoy monitoring stations during tropical cyclone events. Wind speed and significant wave height samples were subjected to Gumbel model fitting and analysis, and location and scale parameters were obtained using Origin 9.0 software (Malekan & Rouhani 2019).

2. RESULTS AND ANALYSIS

2.1. Characteristics of tropical cyclones in Zhejiang

2.1.1. Movement path types

Based on the analysis of tropical cyclone movement path data from 2000 to 2018, a total of 77 tropical cyclones affected the Zhejiang region over the 19-year period. According to the classification of tropical cyclone landfall paths, the tropical cyclones impacting the region can be roughly categorized into four types (Figure 2). Type A: The center of the tropical cyclone makes a direct landfall in Zhejiang; Type B: The tropical cyclone makes landfall along the coast of Fujian and then moves northwest into inland areas; Type C: The tropical cyclone makes landfall along the coast of Fujian and then moves north into Zhejiang and Shanghai areas; Type D: The tropical cyclone closely approaches the coast of Fujian and Zhejiang before turning northward and moving into Northeast Asia. Over the 19-year period, Type D tropical cyclones were the most frequent, totaling 31; Type C tropical cyclones were the least frequent, with 10 occurrences; Type A and Type B tropical cyclones had 18 occurrences each.

2.1.2. Temporal characteristics

On average, about four tropical cyclones enter the impact area each year (Figure 3). The annual count of tropical cyclones exhibits considerable variability, with the highest occurrence being 7 in 2018, and the lowest occurrences, with only two tropical cyclones, in the years 2003, 2009, 2010, 2011, and 2014.

Tropical cyclone activity occurs predominantly from May to October, with a peak in activity from July to September. August has the highest occurrence of tropical cyclones, with 24 instances, while May has the fewest occurrences, with only 1 instance. No tropical cyclones entered the impact area during the months of January to April and November to December.

For Type A tropical cyclones, the peak of impact occurs in August; for Type B, the peak occurs in July to August; for Type C, the peak impact is in July; and for Type D, there are two impact peaks, one in June and another in September.

2.1.3. Intensity characteristics

The variation in tropical cyclone accumulated cyclone energy (ACE) reflects the overall trend in the total energy of tropical cyclone activity (Figure 4). Over the 19-year period, the total ACE value for tropical cyclones entering the impact area was 255.49×10^4 m^2/s^2, with an annual average ACE value of $(13.45 \pm 0.11) \times 10^4$ m^2/s^2. The annual ACE values for the impact area exhibited a decreasing trend during 2000–2003 and 2005–2010, while a fluctuating increasing trend was observed during 2011–2018.

The monthly ACE values of tropical cyclones in the impact area show clear seasonal variation. ACE values increase month by month from May to August, with the largest increases occurring in July and August. The maximum ACE value was 70.24 × 10^4 m^2/s^2 in August, while ACE values decreased from September to October.

Among the different types of tropical cyclones, Type D had the highest total ACE value of 95.52 × 10^4 m^2/s^2, while Type C had the lowest total ACE value of 27.44 × 10^4 m^2/s^2. The total ACE values for Type A and Type B were 35.22 × 10^4 m^2/s^2 and 54.90 × 10^4 m^2/s^2, respectively. The peak ACE values for each type of tropical cyclone occurred at different months. For Type A, the peak ACE occurred in August; for Type B, it occurred from July to September; for Type C, it occurred in August; and for Type D, it occurred in September.

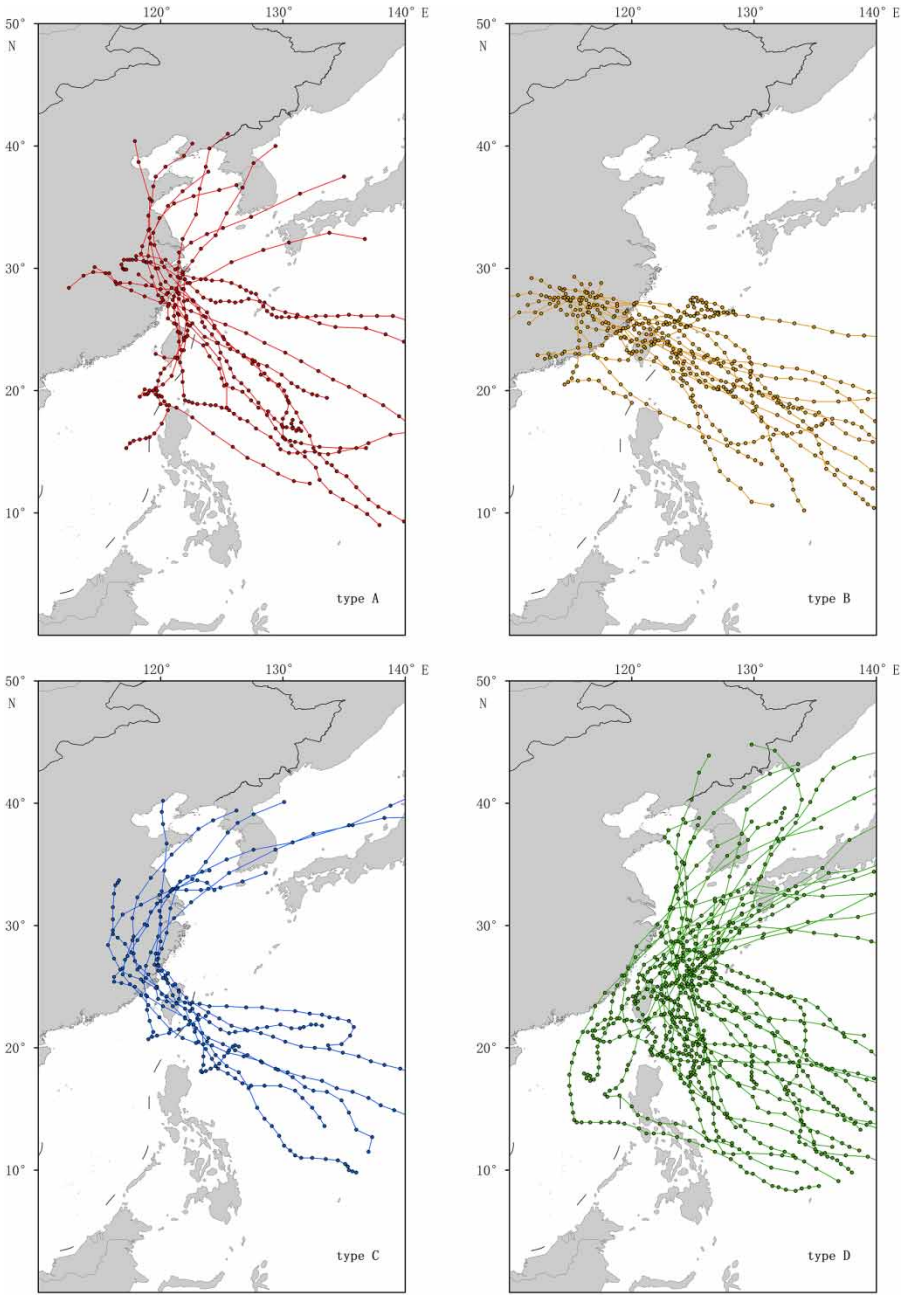

Figure 2 | Four typical paths of tropical cyclones affecting the Zhejiang coastal area from 2000 to 2018.

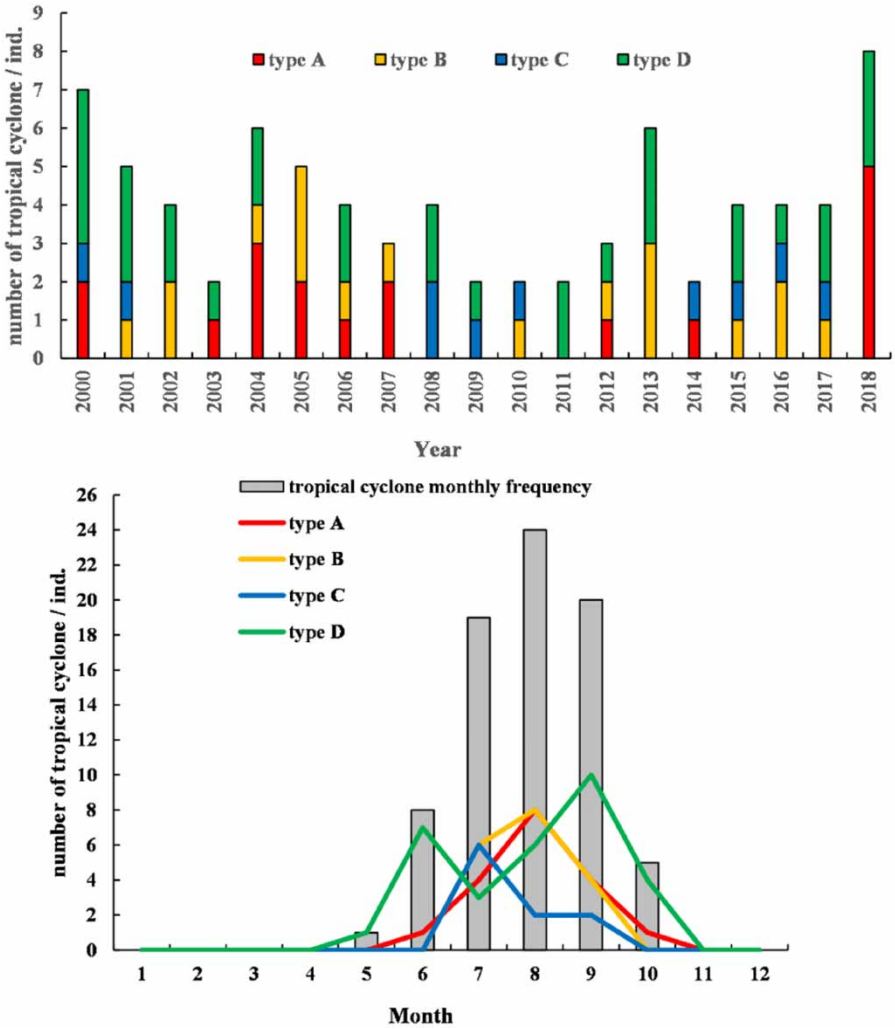

Figure 3 | Tropical cyclone yearly and monthly frequency time series in the Zhejiang coastal area from 2000 to 2018.

2.2. Mussel aquaculture variations affected by tropical cyclone

The data on the area and production of mussel aquaculture in Shengsi County, based on the Zhoushan Statistical Yearbook released by the Zhoushan Statistical Bureau from 2002 to 2018, were used to plot the annual curve of mussel aquaculture area and production in Shengsi (Figure 5(a)). During the period from 2003 to 2010, the mussel aquaculture area and production in Shengsi increased annually, with an average annual growth rate of 14.20% in the aquaculture area and 10.36% in production. In 2010, the aquaculture area reached a maximum of approximately 1,614 ha, with a production of 78,800 tons. In 2011, both aquaculture area and production sharply declined. The aquaculture area decreased to 1,003 ha, and the production was 47,600 tons, representing a 39.03 and 39.61% decrease, respectively, compared to 2010. From 2012 to 2018, the aquaculture area and production gradually recovered, with average annual growth rates of 6.68 and 15.07%, respectively. Notably, in the period from 2016 to 2017, despite a modest increase of 4.16% in the aquaculture area, the production growth rate surged to 24.69%, resulting in a unit area yield of 100.66 tons/hectare.

According to the information on losses in Shengsi mussel aquaculture due to tropical cyclone disasters from 2007 to 2018, obtained from Shengsi County's National Economic and Social Development Statistical Bulletin, Zhoushan Daily, and the Zhejiang Fisheries Mutual Insurance Association: (a) In August 2011, Typhoon 'Muifa' ravaged Shengsi in Zhoushan, causing a complete loss of mussel cultivation in 706.67 ha in Gouqi Township. The direct economic loss exceeded 2 billion yuan. (b) In August 2012, Typhoon 'Haikui' made landfall in Xiangshan, Zhejiang. The northern mussel cultivation area in Gouqi

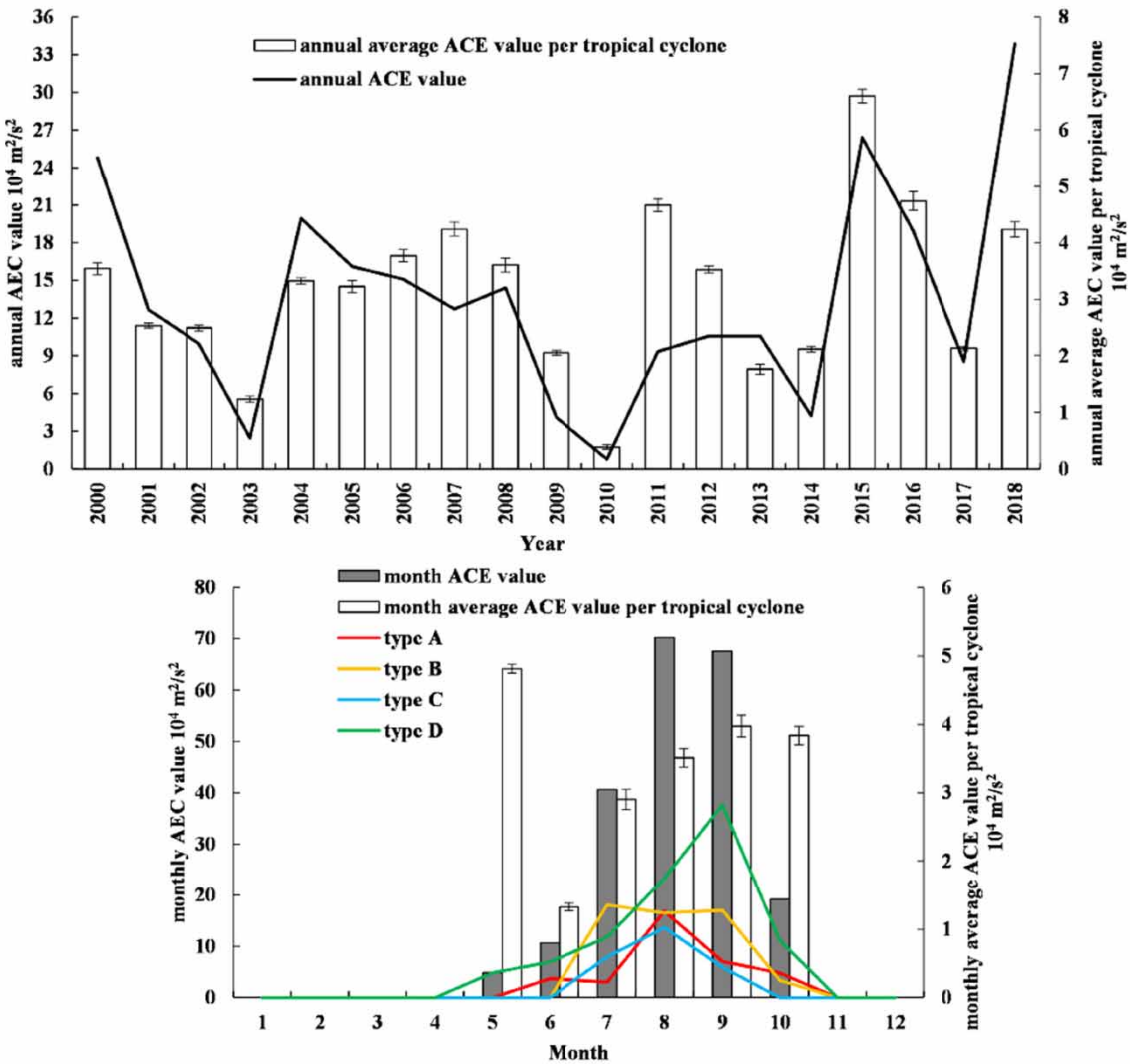

Figure 4 | Annual and annual average per tropical cyclone accumulated cyclone energy value in the Zhejiang coastal area from 2000 to 2018.

Township was slightly damaged, with some mussels shedding near the sea surface (20–30 cm). The southern cultivation area suffered minor damage. (c) In July 2015, Typhoon 'Chanhom' directly hit Shengsi, causing almost all mussel cultivation rafts in Lixi Village and Miaogan Village, as well as in Longquan Village and Shipu Village in Ma'an Archipelago, to overturn. The direct economic loss reached 4 billion yuan. (d) In September 2017, Typhoon 'Talim' approached, leading mussel aquaculturists in Shengsi to harvest nearly 3,000 tons of mussels in anticipation. After the typhoon, all aquaculture rafts in the southeast cultivation area of Gouqi Township were overturned. (e) In July 2018, the Zhejiang Fisheries Mutual Insurance Association received 123 claims related to Typhoon 'Ampil,' of which 80 were for Shengsi mussel aquaculture mutual insurance, covering incidents of mussel shedding.

Based on the data of the mussel aquaculture area and production in Shengsi County, the annual unit area yield is obtained (Figure 5(b)). Pearson correlation analysis was conducted between the annual unit area yield of mussel aquaculture in Shengsi County and the Annual Cyclone Energy index of the strongest tropical cyclone in the cultivation area. The results of the correlation test indicate a highly significant negative correlation between the two variables ($r = -0.813$, $p = 0.002$).

During the period from 2004 to 2008, the unit area yield exhibited a declining trend, decreasing from 54.97 tons/ha in 2003 to 38.77 tons/ha in 2008. Concurrently, the ACE of the strongest tropical cyclone in each year increased annually, rising from 2.07×10^4 m^2/s^2 in 2004 to 4.73×10^4 m^2/s^2 in 2008. With the reduction in ACE in 2009 and no tropical cyclone affecting

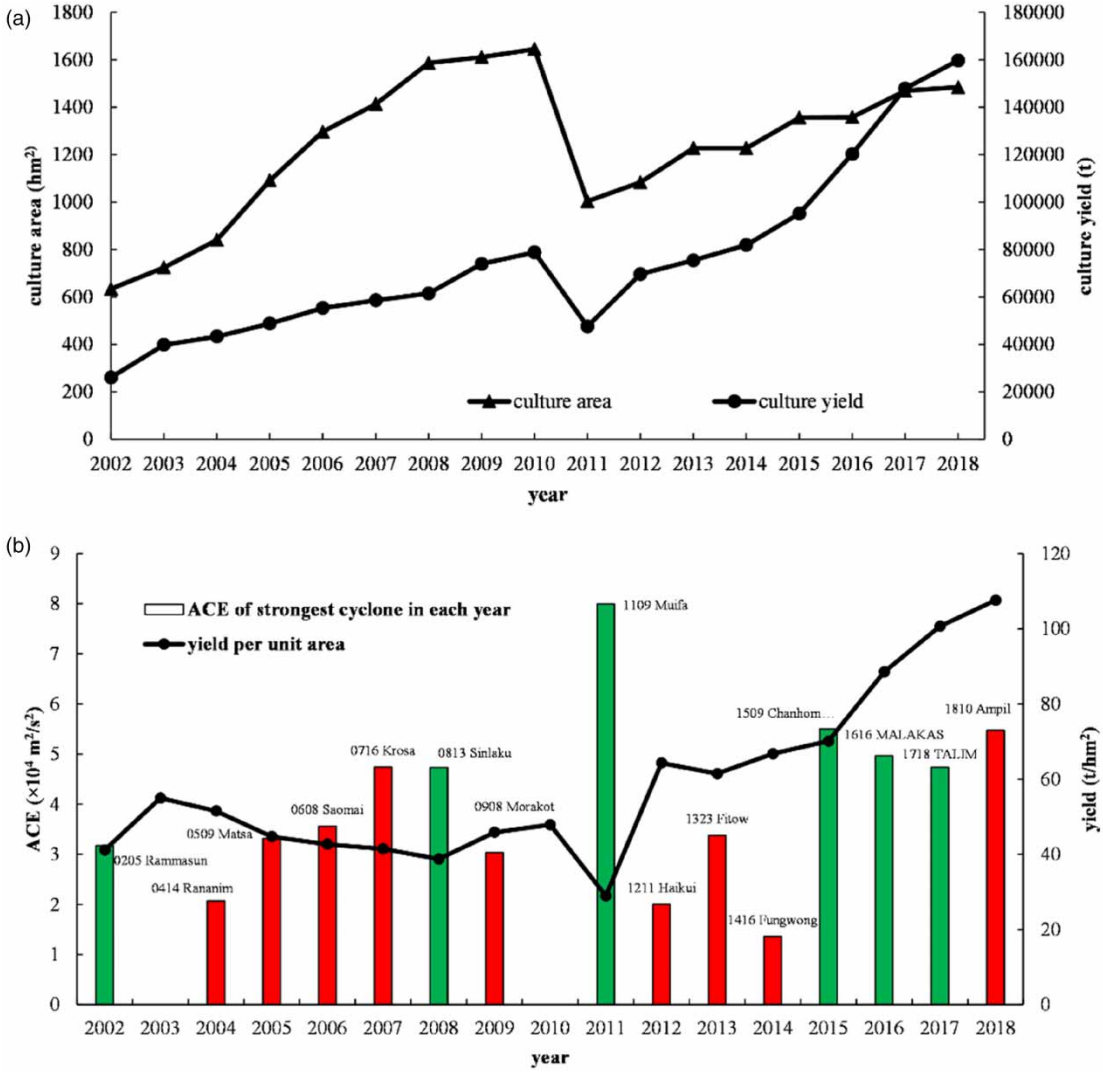

Figure 5 | Culture area and yield (a), the relative rate of yield per unit area and ACE of the strongest cyclone and (b) in Shengsi mussel culture area. *Note:* red bar for type A tropical cyclone, green bar for type D tropical cyclone.

the area in 2010, the unit area yield gradually increased from 2009 to 2010. In 2011, the mussel aquaculture area in Shengsi encountered the strongest tropical cyclone Muifa with an ACE of 8.00×10^4 m^2/s^2 in nearly 17 years, leading to a sharp decrease in unit area yield, reaching only 28.92 tons/hectare. Since 2011, from 2012 to 2014, when the ACE of tropical cyclones in the Shengsi mussel aquaculture area was relatively low, the unit area yield remained at the level of 64.18 tons/hectare.

2.3. Environmental factor characteristics and distribution

2.3.1. Wind field

As the center of a tropical cyclone gets closer to the study area, the wind speed gradually increases (Figure 6). The maximum wind speed also reaches its peak when the center of the tropical cyclone is closest to the study area. A linear correlation analysis between these two variables shows a highly significant negative correlation ($r = -0.334$, $p < 0.01$).

The closest distance of a tropical cyclone to the study area is 105.38 km. The influence of a tropical cyclone on the wind speed in the Shengsi Marine Ranch has a certain range, with a significant difference in maximum wind speed observed between the distance range of 400–450 km ($F = 56.421$, $p < 0.01$).

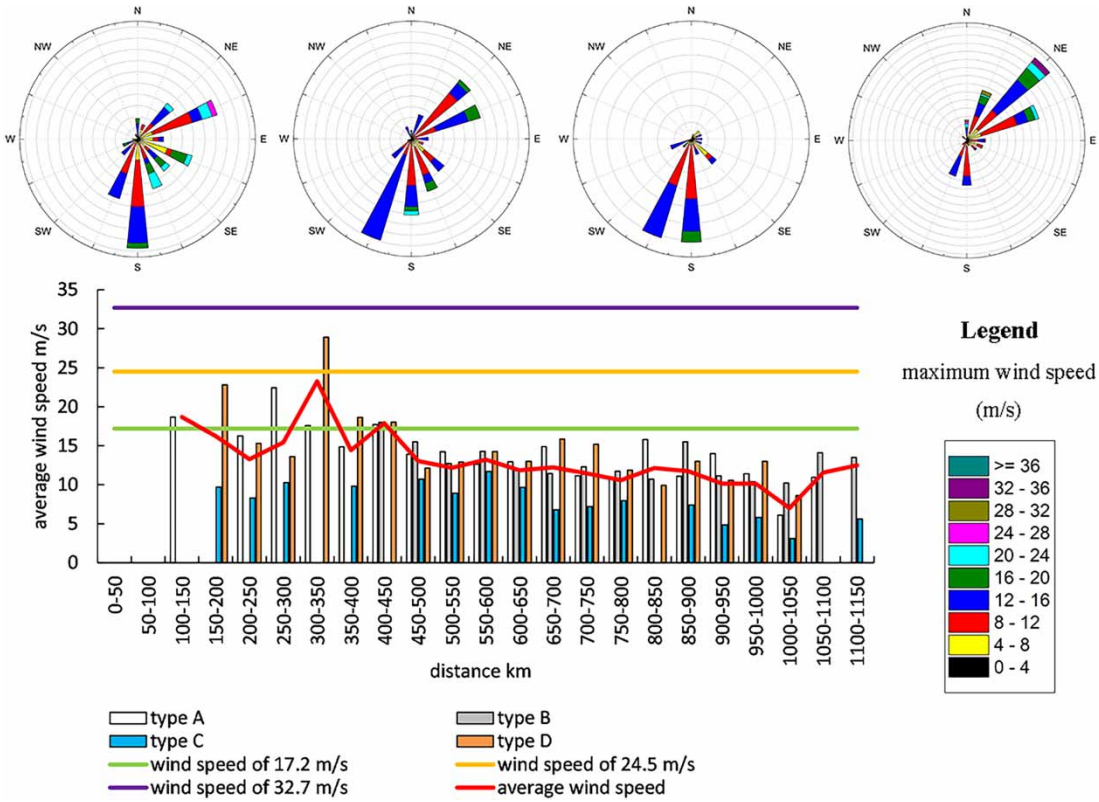

Figure 6 | Relationship between maximum wind speed, the direction in Shengsi marine ranching under different types of tropical cyclones and the distance from tropical cyclone center.

Different types of tropical cyclones have varying degrees of impact on the wind field in the Shengsi Marine Ranch area. Tropical cyclones of Type A and Type D are responsible for generating winds of Beaufort scale 8 (17.2 m/s) or higher, while only Type D tropical cyclones cause winds of Beaufort scale 10 (24.5 m/s) or higher in the marine ranch area.

2.3.2. Significant wave height

As the center of a tropical cyclone gets closer to the study area, the average significant wave height gradually increases (Figure 7). There is a highly significant negative correlation between these two variables ($r = -0.733$, $p < 0.01$). The influence of tropical cyclones on the average significant wave height in the Shengsi Marine Ranch has a certain range, with a significant difference in average significant wave height observed in the range of approximately 650 km ($F = 6.161$, $p = 0.002$).

Significant differences exist in the distribution of average significant wave height among different types of tropical cyclones and non-cyclone impact periods within the range of 0–650 km ($F = 8.906$, $p < 0.01$). During non-cyclone impact periods, the average significant wave height in the study area is 0.94 ± 0.40 m, predominantly from the south. Among the four types of tropical cyclones, Type D has the highest average significant wave height, reaching up to 6.51 m, with an average of 1.50 ± 0.83 m. The wave direction is mainly from northeast–east, with the predominant direction being northeast–east. Type A tropical cyclones have the second highest average significant wave height, reaching up to 5.96 m, with an average of 1.47 ± 0.88 m. The wave direction is mainly from east–southeast, with the predominant direction being southeast–east. Type B tropical cyclones exhibit slightly higher significant wave heights compared to non-cyclone impact periods, with a broad distribution of wave directions, predominantly from southeast–south. The distribution of significant wave height for Type C tropical cyclones is consistent with that of non-cyclone impact periods, with a shift toward an eastward wave direction, primarily from south–southeast.

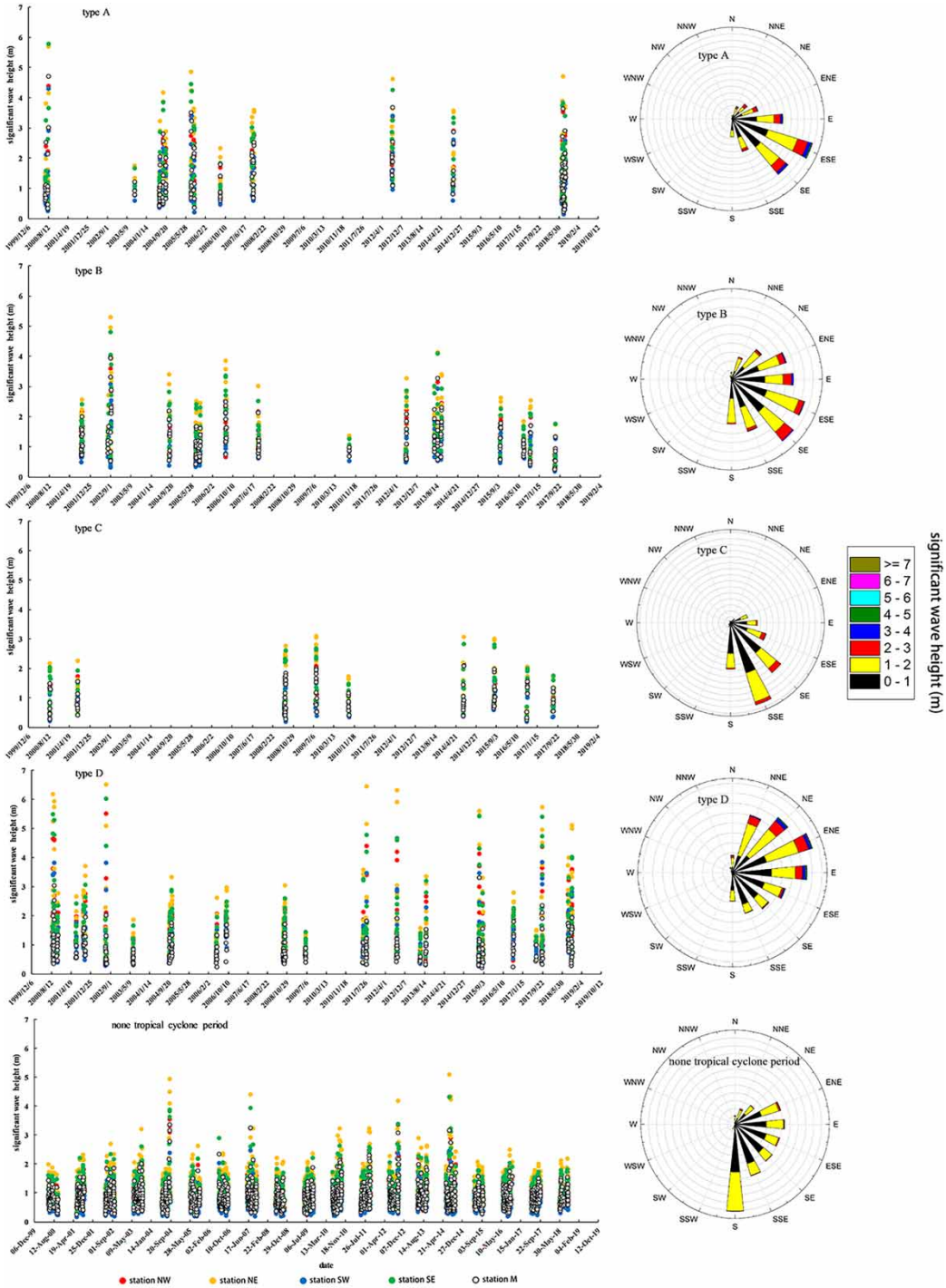

Figure 7 | Significant wave height, and direction in Shengsi marine ranching under different types of tropical cyclones.

2.4. Wind and wave joint probability distribution model

2.4.1. Marginal distribution and testing

Suppose there is a set of sub-samples arranged in ascending order as (x_1, x_2, ..., x_i, ..., x_N). For any real number x_i ($1 \leq i \leq N$), according to reference (Yue *et al.* 1999), the empirical cumulative probability that the random variable X does not exceed x_i

can be obtained by the following formula:

$$F^*(x_i) = P_i(X \le x_i) = \frac{i - 0.44}{N + 0.12} \tag{10}$$

where N is the sub-sample size. Equation (10) provides an unbiased estimate of the cumulative probability distribution for wind speed and significant wave height.

The Kolmogorov–Smirnov test method was employed to verify whether the marginal distributions of wind speed and significant wave height conform to the Gumbel distribution (Nie *et al.* 2014). The results indicate that there is a significant level in the marginal distributions of wind speed and significant wave height ($p = 0.0027$ and $p = 0.0043$), as confirmed through hypothesis testing (Figure 8).

2.4.2. Parameter estimation and functions

From a perspective encompassing biology, ecology, and environmental science, this paper determines the distribution parameter estimates of the joint probability distribution through the marginal distribution of variables. This involves employing methods such as the moment method, maximum-likelihood method, probability weighting method, etc., to estimate parameters of their marginal distributions. Consequently, the corresponding parameter estimates for the joint probability distribution are established. Following the ideas proposed by Gumbel & Mustafi (1967), the moment method is recommended for estimating parameters that express the degree of correlation, which is applied using Equations (3) and (4) to estimate the parameters reflecting the degree of correlation. For the location parameters and scale parameters of the marginal distributions, the probability weighting moment method is employed for estimation. The results of each parameter estimate are presented in Table 1.

Substituting the parameter estimates into Equations (7)–(9), we obtain the marginal distribution functions for annual extreme wind speed and significant wave height, as well as the joint probability density function and joint return period function.

The marginal distribution functions for wind speed and significant wave height are given by:

$$\begin{cases} F_X(x) = \mathrm{e}^{-[e^{-0.2977(x-15.3126)}]} \\ F_Y(y) = \mathrm{e}^{-[e^{-0.8625(y-3.7006)}]} \end{cases} \tag{11}$$

The joint cumulative probability distribution function for wind speed and significant wave height is given by:

$$F_{XY}(x, y) = \mathrm{e}^{-[e^{-0.6467(x-15.3126)} + e^{-1.8733(y-3.7006)}]^{0.4604}} \tag{12}$$

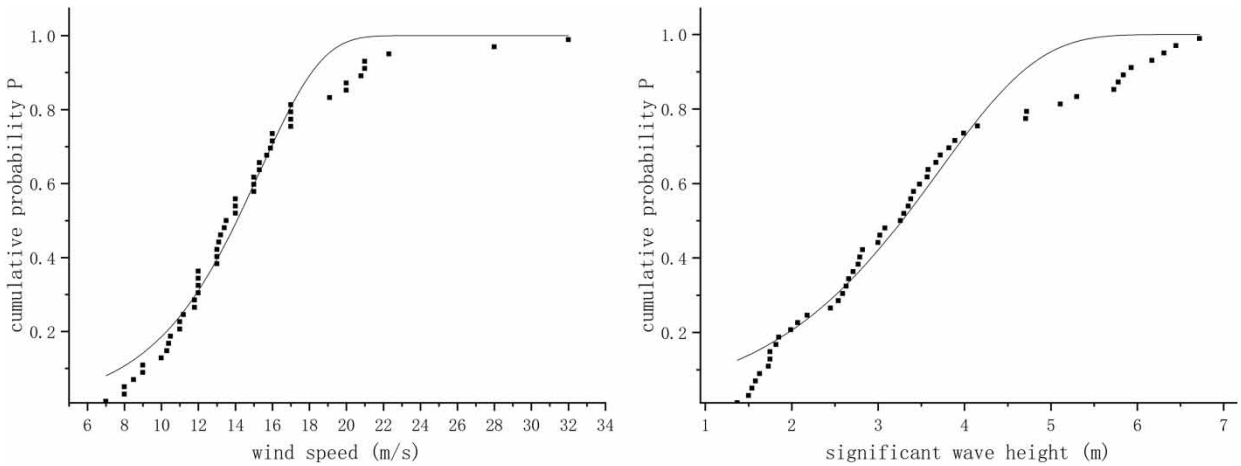

Figure 8 | Wind speed and significant wave height marginal distribution.

Table 1 | Estimation of marginal distribution parameters and correlation factors

Marginal variable	Location parameter	Scale parameter	Correlation coefficient	Correlation parameter
Wind speed (x)	15.3126	3.3587	0.7880	2.1719
Significant wave height (y)	3.7006	1.1594		

The joint return period function for wind speed and significant wave height is:

$$T_{XY} = \frac{1}{1 - \mathrm{e}^{-[e^{-0.6467(x-15.3126)} + e^{-1.8733(y-3.7006)}]^{0.4604}}} \tag{13}$$

The variables in the equations are as follows: x represents the wind speed (m/s), and y represents the significant wave height (m).

The joint distribution function, joint probability density function, and joint return period function for annual extreme wind speed and significant wave height are valuable in practical applications for determining the design wind speed and effective wave height loads on aquaculture rafts. They provide combinations of wind speed and significant wave height corresponding to a specific probability or return period, allowing for the rational determination of design loads on aquaculture raft structures. This is something that cannot be achieved with univariate extreme value distributions.

2.4.3. Model statistical testing

To verify the applicability of the Gumbel logic model to the joint distribution of wind speed and significant wave height, as well as to assess the differences between observed and theoretically simulated joint cumulative probabilities, a variance test was conducted on the calculated results of observed and simulated theoretical joint cumulative probabilities (Figure 9). The results indicated no significant differences ($F = 0.786$, $p = 0.378$). Hence, it can be inferred that the derived model is suitable for representing the joint distribution of maximum wind speed and significant wave height under the influence of tropical cyclone activity in the study area of Shengsi Ma'an Archipelago.

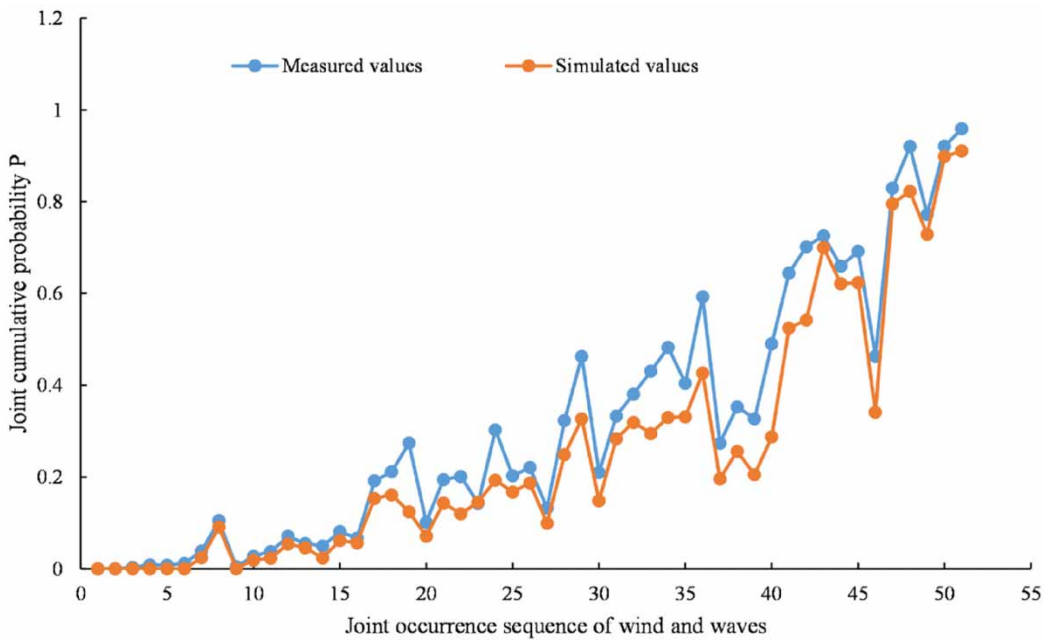

Figure 9 | Measured probability and simulated probability of joint distribution of wind speed and significant wave height.

2.4.4. Variation in return period wind speed and significant wave height

Based on the observed samples of wind speed and significant wave height, the calculated results for the corresponding return periods are presented in Table 2. Since the year 2000, Shengsi-Ma'anshan Marine Ranch has experienced the strongest tropical cyclone, Muifa as indicated by the results in Table 2. The wind and wave conditions generated by Muifa are greater than those of a 'once-in-ten-years' event. If tropical cyclone activity leads to wind and wave conditions occurring with a return period of 'once-in-three-years' in the study area, then the wind speed in the study area needs to reach 20 m/s, approximately equivalent to a Beaufort scale wind level of 8, and the significant wave height should reach 4.71 m, roughly corresponding to a wave level of 6. If tropical cyclone activity results in wind and wave conditions with a return period of 'once-in-ten-years' in the study area, then the required wind speed is 28 m/s, approximately equivalent to a Beaufort scale wind level of 10, and the significant wave height needs to reach 6.31 m, roughly corresponding to a wave level of 7.

3. DISCUSSION

3.1. Temporal and spatial patterns of tropical cyclones

June to November is the typhoon season in China, especially during the summer and early autumn months of July to October when typhoon activity is most frequent and concentrated. For the purpose of substantiating and elaborating upon the claim of north to south variation in tropical cyclone activity over China, a north-to-south anti-correlation in yearly activity is confirmed in the historical cyclone records. A similar spatial variation is identified in the modern records using a factor analysis model, which delineates typhoon activity over the southern provinces of Guangdong and Hainan from the activity over the northern provinces of Fujian, Taiwan, Zhejiang, Shanghai, Jiangsu, and Shandong (Fogarty *et al.* 2006).

In this study, there are variations in the activity time, paths, and intensity of tropical cyclones, showing a northward migration over time. Type B tropical cyclones peak in influence from July to August, Type A peaks from August to September, and September is the peak for Type D tropical cyclones. Combining the spatial distribution of tropical cyclones with B → A → D types, the movement path of tropical cyclones shifts northward as time progresses. Although August has the highest number of tropical cyclones, and the total ACE is also the largest in that month, the average ACE of tropical cyclones is highest in September. This indicates that tropical cyclone activity in September is the most active and has higher intensity in the study area. From October onwards, the number of tropical cyclones in the study area sharply decreases, and their intensity decreases as well.

The spatial and intensity variations of tropical cyclones are mainly influenced by various factors such as geographical location, oceanic environment, and meteorological conditions (Skok *et al.* 2013). The formation and sustenance of tropical cyclones require warm and humid conditions, with warm sea-surface temperatures being a crucial factor in the formation and

Table 2 | Distribution of wind speed and significant wave height in different recurrence periods

Recurrence period (year)	Wind speed (m/s)	Beaufort scale	Significant wave height (m)	Wave scale	*p*
2.10	15.9	7	5.73	6	0.702
2.18	17	7	5.3	6	0.726
2.64	20	8	4.72	6	0.659
2.65	17	7	6.17	7	0.692
3.33	20	8	4.71	6	0.463
3.68	21	9	6.72	7	0.830
4.89	22.3	9	5.11	6	0.920
5.64	21	9	5.93	6	0.772
9.85	28	10	6.31	7	0.921
11.20	32	11	6.45	7	0.948
20[a]	35	12	7.15	8	0950
50[a]	40	13	8.22	8	0980
100[a]	45	14	9.08	8	0990

[a]The predicted value of the recurrence period.

intensification of typhoons (Cao *et al.* 2021). The waters in the Zhejiang Sea area usually have higher temperatures only during the summer and early autumn, providing a warm oceanic environment for tropical cyclones. The warm sea-surface temperature supplies sufficient warm and moist air to the atmosphere, providing energy for the tropical cyclones, and facilitating their formation and intensification.

The spatiotemporal characteristics of the tropical cyclone movement path are primarily influenced by large-scale oceanic and weather systems (Huang & Xu 2009). Vertical wind shear plays a crucial role in the formation and maintenance of typhoons, with smaller vertical wind shear aiding in maintaining the vertical symmetry of the cyclonic structure. In the Zhejiang Sea area, there are seasonal variations in the monsoon during the summer and autumn, where the oceanic monsoon can reduce vertical wind shear. Additionally, the movement of subtropical high-pressure systems, such as upper-level troughs and ridges, can also impact vertical wind shear (Lai *et al.* 2020). The strength of subtropical highs can affect the east–west movement of tropical cyclones (Ni *et al.* 2013). Therefore, the variations in these vertical wind shear systems contribute to the spatial distribution pattern of the B → A → D type tropical cyclone paths observed in this study.

3.2. Relationship between tropical cyclone activity and climate change

Previous research has indicated a close relationship between tropical cyclones and El Niño and La Niña events (Elsner & Kocher 2000). El Niño and La Niña are large-scale sea-surface temperature anomalies in the Pacific Ocean, and they have widespread and significant impacts on global climate, including the regulation of tropical cyclone activity (Ramsay *et al.* 2011). Patricola *et al.* (2022) investigated years when observed global typhoon activity deviated from the mean and its potential associations with oceanic drivers from 1980 to 2021. La Niña and positive Atlantic Multidecadal Oscillation (AMM) were correlated with the bottom percentiles of two typhoon indices, while El Niño and negative AMM showed the opposite pattern. Tu *et al.* (2019) studied the decadal and interannual variations in the meridional tropical cyclone activity around Taiwan in the northwest Pacific after 1998 from September to October. For interannual variations, the frequency of typhoon passages in the northwest Pacific around Taiwan tended to decrease during El Niño events and increase or decrease during La Niña-related events. According to the studies by Liu *et al.* (2017) and Qin *et al.* (2015), the years 2002, 2004, 2008, and 2014–2016 were El Niño years. In this study, the number of tropical cyclones in 2003, 2009–2011, and 2014 was lower than usual, with only two tropical cyclones recorded in each of these years. He *et al.* (1999) found that under the influence of El Niño, the occurrence of tropical cyclones is suppressed, and sometimes the suppression can lead to changes in the number of tropical cyclones in the following year. The anomalous number of tropical cyclones in 2003 and 2009 in this study occurred after the strong El Niño events in 2002 and 2008, consistent with the analysis and predictions of relevant scholars.

The El Niño event significantly influences the intensity of tropical cyclones. The El Niño event leads to an increase in sea-surface temperatures in the tropical Pacific region, potentially providing more favorable conditions for the formation and intensification of tropical cyclones. Warm sea waters typically supply more energy to cyclones, making them more likely to develop into strong storms (McInnes *et al.* 2016). Using a stochastic cyclone simulation method, the probability of storm tides (a combination of storm surges and astronomical tides) in Samoa was assessed. Under El Niño conditions, the frequency of typhoons and storm tides is similar to the frequency across all seasons, but it is significantly lower during La Niña conditions. The El Niño event can cause anomalous changes in atmospheric circulation, which has important implications for the paths and intensities of tropical cyclones. Lyon & Camargo (2009) studied the seasonal evolution of anomalous atmospheric circulation over the northwest Pacific during El Niño and La Niña and placed these features in the context of the large-scale evolution of El Niño-Southern Oscillation (ENSO) events, including an analysis of changes in tropical cyclone activity affecting the northwest Pacific. These changes may involve variations in wind shear, affecting the vertical development of cyclones.

In this study, the ACE values of tropical cyclones exhibit interannual fluctuations, and the changing trend aligns with the impact of El Niño years on the variation in the number of tropical cyclones. Under the influence of El Niño, during the years 2011, 2015, and 2016, even though the number of tropical cyclones was not high, and the total ACE values for the year were not substantial, the average ACE value for individual tropical cyclones in those years was higher compared to other years. This suggests that the tropical cyclones generated in these years had higher intensity. Examples include Typhoon Muifa in 2011, Typhoon Chanhom in 2015, and Typhoon Meranti in 2016 (Chen *et al.* 2013; Liu *et al.* 2013; Duan *et al.* 2017; Yan *et al.* 2019).

The elevated sea temperatures provide more energy for tropical cyclones, making it easier for them to develop into intense storms. El Niño can lead to significant changes in atmospheric circulation, affecting the paths of tropical cyclones and making certain regions more susceptible to the impact of these cyclones. Strong El Niño events may cause alterations in

atmospheric wind shear (changes in vertical wind speed), reducing wind shear and potentially making it easier for tropical cyclones to form and intensify. Therefore, during El Niño years and especially after strong El Niño events, it is crucial to pay attention to the disaster impact caused by the formation of tropical cyclones.

3.3. Analysis of the response of tropical cyclone activity to wind waves in aquaculture areas

The impact of tropical cyclones on wind speed in the Shengsi mussel culture area is most extensive for Type D tropical cyclones, with the greatest intensity. This is followed by Type A tropical cyclones, while Types B and C tropical cyclones have a smaller impact. Type D tropical cyclones have repeatedly recorded average wind speeds of 30 m/s within a range of 450 km from the Shengsi mussel culture area. This is mainly attributed to cyclones like Prapiroon and Muifa directly passing through the southeast or east seas of the Shengsi mussel culture area (Hu 2001; Sha *et al.* 2003; Wu *et al.* 2007; Huang *et al.* 2016).

In contrast, Type A tropical cyclones have a relatively smaller impact on wind speeds in the Shengsi mussel culture area compared to Type D tropical cyclones. This is because Type A tropical cyclones affect the sea areas of the Shengsi mussel culture area from the land to the east. By this time, the cyclone intensity has significantly weakened to the level of a severe tropical storm or similar intensity (Liu *et al.* 2007; Wang *et al.* 2018).

The wind directions generated by the two types of tropical cyclones are different, with Type A cyclones having a southward bias, while Type D cyclones have a northeastward bias. Therefore, the effective wave height driven by the wind will exhibit different characteristics. The order of the impact of the effective wave height on the sea area of the Shengsi mussel culture area from large to small is Type D > Type A > Type B > Type C, corresponding to changes in the average effective wave height and wave direction from northeast–east (Type D), southeast–east (Type A), south–southeast (Type B), and south–southeast (Type C).

Under the influence of tropical cyclones, the effective wave height in the sea area of the Shengsi mussel culture area is generally distributed with higher values to the east and lower values to the west. This is related to the arcuate distribution of the Ma'an Archipelago, especially the geographical distribution of islands such as Huaniao Island, Bi Xia Shan Island, and Sheng Shan Island, which play a crucial role in blocking waves in the east seas of the Ma'an Archipelago (Zhou *et al.* 2014). Therefore, relevant management authorities and personnel in the Shengsi mussel culture area should pay special attention to the activity changes of Type D tropical cyclones during disaster prevention and reduction, aiming to reduce losses in mussel farming.

3.4. Joint wind-wave distribution and mutual insurance for scallop aquaculture

Tropical cyclone, a high-energy destructive meteorological system with heavy rainfall and gale-triggered massive landslides and windstorms, poses a significant threat to coastal areas. Xiao *et al.* (2011) developed a tropical cyclone potential impact index (TCPI) based on the air mass trajectories, disaster information, intensity, duration, and frequency of tropical cyclones. These skillfully estimate the mean seasonal variation of observed cyclones, but they struggle with reproducing interannual frequency variability and change. The joint distribution function, joint probability density function, and joint return period function of annual extreme wind speeds and significant wave heights are highly useful in determining the design loads of wind speed and significant wave height for the construction of mussel farming facilities. They can provide combinations of wind speeds and significant wave heights corresponding to a specific probability or return period. This allows for the rational determination of design wind speed and significant wave height loads for mussel farming facilities, a task that cannot be achieved with univariate extreme value distributions.

In 2018, the mussel farming area in Shengsi had a total area of approximately 1486.67 ha, producing about 159,700 tons of mussels with an annual output value of 447 million yuan (Zhoushan Bureau of Statistics 2018). Throughout the history of mussel farming in Shengsi, significant losses have occurred multiple times due to tropical cyclone disasters. To address this, various departments jointly formulated and implemented mutual assistance insurance for mussel farming in Shengsi to safeguard the livelihoods of fishermen after disasters (Pan & Wu 2012).

According to the pilot implementation plan for aquaculture mutual assistance insurance in Zhejiang Province released in 2017, the triggering point for compensation is defined as wind disasters of magnitude 10 or above (24.5 m/s) and storm surges caused by such events, as well as waves exceeding 3 m. The compensation standards are detailed in Table 3 (He 2019). Based on the distribution of the return period of wind and waves at the compensation base point, it can be inferred that the

Table 3 | Compensation standards of Shengsi mussel culture insurance

Compensation ratio %		Wave height H (m)			
		$3.0 \leq H < 5.0$	$5.0 \leq H < 7.5$	$7.5 \leq H < 11.5$	$11.5 \leq H$
Wind scale	10–11	50	60	80	90
	12–13	60	75	90	100
	14–15	80	90	100	100
	≥16	90	100	100	100

threshold for payouts in the mutual assistance insurance for mussel farming in Shengsi is relatively low as a social assistance mechanism for livelihood protection. However, meeting the conditions for a high payout ratio remains relatively challenging.

According to the tropical cyclone movement warning and forecast path records released by the China Meteorological Administration (https://tcdata.typhoon.org.cn/zjljsjj.html) in 2019, a total of six tropical cyclones entered the impact area, and 2019 was an El Niño year. Meanwhile, based on the recurrence characteristics of tropical cyclone activity in the Ma'an Archipelago region in this study, the highest-intensity tropical cyclone, Muifa, has a recurrence period of 11.20 years. Since Muifa, during the years 2020 and the following 1–2 years, tropical cyclones of this intensity have recurred in the Ma'an Archipelago region. Therefore, in the context of this study, the number of tropical cyclones occurring in the Ma'an Archipelago region in 2020 or the next 1–2 years may be fewer than in 2018–2019, but the individual tropical cyclones are likely to exhibit higher intensity.

According to the tropical cyclone movement warning and forecast path records released by the China Meteorological Administration (https://tcdata.typhoon.org.cn/zjljsjj.html) from 2020 to 2022, there were four tropical cyclones entering the impact area in 2020, three in 2021, and five in 2022. Among them, the Zhejiang Fisheries Mutual Aid Association's aquaculture mutual insurance revealed the payout situation in 2021 (https://www.zfmi.com/zfmi/cats/xxgk.pkgs.html): severe Typhoon 'In-Fa' caused severe damage to the ShiPu, LiXi, and HouLongTou areas of Shengsi Gouqi Township, with some areas suffering complete destruction. A total of 136 aquaculture households claimed damages, and the claims amounted to over 11.3 million yuan. In 2022, the super typhoon Chanthu lingered in the eastern sea area of Shengsi, bringing significant impact to the Shengsi scallop aquaculture industry. The scallop aquaculture suffered severe damage, with reported damaged areas covering approximately 4,000 acres, resulting in insurance payouts of around 21.23 million yuan. The decrease in the number of tropical cyclones and the occurrence of intense tropical cyclones, such as In-Fa and Chanthu in 2021, during the period from 2020 to 2022, are consistent with the recurrence characteristics and warnings of tropical cyclone activity simulated in the Ma'an Archipelago region as indicated in this study.

Therefore, the wind-wave joint probability distribution model constructed for the Shengsi Ma'an Archipelago area in this study possesses a certain degree of accuracy and practicality. Based on this, it is recommended that the Shengsi Ma'an Archipelago area should make adequate preparations for tropical cyclone disasters in the years following strong El Niño events. The Shengsi mussel farming mutual aid insurance should also play an active role. With the increase in the number of insured members and insurance funds, the Shengsi mussel farming mutual aid insurance can lower the conditions for payout ratios, expand the coverage, and achieve a risk protection service for mutual assistance among farmers.

4. CONCLUSION

(1) During the 19-year period, a total of 77 tropical cyclones affected Zhejiang, categorized into four types based on their movement paths. Among these, the D-type tropical cyclones were the most numerous, followed by the A-type cyclones. During the study period, there was a regular fluctuation in the annual frequency of tropical cyclones and the Accumulated Cyclone Energy. The prevalent period for tropical cyclones in Zhejiang occurred from July to September, with August having the highest number of cyclonic activities. The most active and energetically intense month for tropical cyclone activity in the region influencing the Shengsi mussel culture area was September. The tropical cyclones affecting the Shengsi mussel culture area were mainly associated with A-type and D-type movement paths, with their activity concentrated in the months of August and September.

(2) D-type tropical cyclones have the widest range of influence on wind speeds in the Shengsi mussel culture area, with the highest impact intensity. A-type cyclones follow, while B and C-type cyclones have a smaller impact. As the center of

tropical cyclones approaches the Shengsi mussel culture area, there is a gradual increase in significant wave height, and the wave direction changes from south to northeast. There is a significant negative correlation between the average distance from the center of the cyclone to the Shengsi Ma'an Archipelago area and the corresponding mean values of wind speed and significant wave height.

(3) In the Shengsi mussel culture area, extreme wind speeds and significant wave heights during tropical cyclone events follow a Gumbel joint probability distribution model. According to the model's prediction, the Shengsi Ma'an Archipelago area is expected to experience tropical cyclones of the intensity level seen in the 2011 Muifa cyclone in 2021. In recent years, it is imperative to prepare for early warning and disaster reduction measures for tropical cyclone disasters following strong El Niño years.

FUNDING

National Natural Science Foundation of China (32201298), the Central Public-Interest Scientific Institution Basal Research Fund (2021T01), and the Technology Development Projects related to the safety of cold sources in nuclear power plants (21FW018).

DATA AVAILABILITY STATEMENT

The original contributions presented in the study are included in the article/Supplementary Material. Further inquiries can be directed to the corresponding author.

CONFLICT OF INTEREST

The authors declare there is no conflict.

REFERENCES

Brown, C. H. 1952 Some structural proteins of *Mytilus edulis*. *Quarterly Journal of Microscopical Science* **93**, 487–502.

Cao, X., Wu, R.-G., Xu, J., Feng, J., Zhang, X.-P., Dau, Y.-F. & Liu, Y.-Y. 2021 Contribution of the intensity of intraseasonal oscillation to the interannual variation of tropical cyclogenesis over the western North Pacific. *Environmental Research Communications* **3**, 031002. doi:10.1088/2515-7620/abed93.

Chao, Y. C., Merritt, M., Schaefferkoetter, D. & Evans, T. G. 2020 High-throughput quantification of protein structural change reveals potential mechanisms of temperature adaptation in *Mytilus mussels*. *BMC Ecology and Evolution* **20**, 28.

Chen, X.-B., Zhou, L., Shi, W.-L., Li, J. & Chen, X. 2013 Characteristics of wave and surge fields of typhoon Muifa. *Advances in Marine Science* **31** (1), 22–30.

China Island Gazetteer Compilation Committee. 2014 *China Island Gazetteer, Volume 1, Zhejiang Province – Northern Part of Zhoushan Archipelago*. Ocean Press, Beijing, China.

Chinese Animal Taxonomy 1997 Invertebrates Volume Twelve. Science Press, Beijing, China.

Duan, J.-J., Qian, Y.-Z., Zhou, F., Fang, Y.-Y. & Guo, J.-M. 2017 Numerical simulation of topographic effect on heavy rainfall in Northeastern Zhejiang caused by typhoon Chan-Hom. *Meteorological Monthly* **43** (6), 686–695.

Elsner, J. B. & Kocher, B. 2000 Global tropical cyclone activity: A link to the North Atlantic oscillation. *Geophysical Research Letters* **27**, 129–132. doi:10.1029/1999GL010893.

Fogarty, E. A., Elsner, J. B., Jagger, T. H., Liu, K.-B. & Louie, K.-S. 2006 Variations in typhoon landfalls over China. *Advances in Atmospheric Sciences* **23**, 665–677.

Gumbel, E. J. & Mustafi, C. K. 1967 Some analysis properties of bivariate extreme distribution. *Journal of the American Statistical Association* **62**, 569–588.

He, H.-L. 2019 Some thoughts on the settlement case of shallow sea shellfish farming. *China Fisheries* **11**, 49–50.

He, M., Song, W.-L. & Chen, X.-F. 1999 Typhoon activity in the Northwest Pacific in relation to El Nino/La Nina events. *Journal of Tropical Meteorology* **15** (1), 18–26.

Hu, Z.-P. 2001 Characteristics and problems as well as recommendation of typhoon 'Paibian', 'Sangmei' in 2000 effecting on Shanghai. *Urban Roads Bridges & Flood Control* **19** (2), 27–31.

Huang, F. & Xu, S.-B. 2009 Characteristics of super typhoon activity over western North Pacific and its relationship with ENSO. *Periodical of Ocean University of China* **39** (5), 883–888.

Huang, Y., Wang, Y.-G. & Cai, Q.-F. 2016 Analysis on rapid intensity change of the environment condition and energy flux driven by the super typhoon Muifa. *Marine Forecasts* **33** (6), 22–31.

Jahnsen-Guzmán, N., Lagos, N. A., Quijón, P. A., Manríquez, P. H., Lardies, M. A., Fernández, C., Reyes, M., Zapata, J., García-Huidobro, M. R., Labra, F. A. & Duarte, C. 2022 Ocean acidification alters anti-predator responses in a competitive dominant intertidal mussel. *Chemosphere* **288**, 132410.

Johnson, N. J. & Kotz, S. 1972 *Distribution in Statistics: Continuous Multivariate Distribution*. John Wiley & Sons, New York, NY, USA and London, UK.

Kong, H., Clements, J. C., Dupont, S., Wang, T., Huang, X., Shang, Y., Huang, W., Chen, J., Hu, M. & Wang, Y. 2019 Seawater acidification and temperature modulate anti-predator defenses in two co-existing *Mytilus* species. *Marine Pollution Bulletin* **145**, 118–125.

Lai, J., Li, C. & Lu, R. 2020 *Considerable Differences of the Interannual Variations for the Tropical Cyclone Landfall Over North and South East Asia in Summer*. doi:10.5194/egusphere-egu2020-3982.

Lin, J., Li, C. Y. & Zhang, S. Y. 2016 Hydrodynamic effect of a large offshore mussel suspended aquaculture farm. *Aquaculture* **451**, 147–155.

Liu, Y.-Y. 2017 Analysis of spatial interpolation methods for meteorological elements anomaly. *Journal of the Meteorological Sciences* **37** (2), 278–282.

Liu, G., Zhang, Q.-Y. & Sun, S.-Q. 2007 A preliminary study on activities of tropical cyclones over the Western North Pacific during the summer in 2006. *Climatic and Environmental Research* **12** (6), 738–750.

Liu, H., Zheng, C.-W., Lin, G., Sun, Y. & Li, J. 2013 Analysis of typhoon wave field by SWAN wave mode. *Marine Forecasts* **30** (3), 46–50.

Liu, Y.-G., Ma, Y.-S. & Liu, Y.-R. 2017 Relationship between first northward-jump of northwest Pacific subtropical high and tropical cyclone thereafter. *Journal of PLA University of Science and Technology (Natural Science Edition)* **18** (2), 156–162.

Lyon, B. & Camargo, S. J. 2009 The seasonally-varying influence of ENSO on rainfall and tropical cyclone activity in the Philippines. *Climate Dynamics* **32**, 125–141. doi:10.1007/s00382-008-0380-z.

Malekan, A. & Rouhani, S. 2019 Model of contact friction based on extreme value statistics. *Friction* **4**, 327–339.

McInnes, K. L., Hoeke, R. K., Walsh, K. J. E., O'Grady, J. & Hubbert, G. 2016 Application of a synthetic cyclone method for assessment of tropical cyclone storm tides in Samoa. *Natural Hazards* **80**, 425–444. doi:10.1007/s11069-015-1975-4.

Ministry of Agriculture and Rural Affairs, Bureau of Fisheries. 2021 National fishery economic statistical bulletin for the year 2020. *China Fisheries* **549** (8), 11–12.

Moyen, N. E., Somero, G. N. & Denny, M. W. 2020 Mussel acclimatization to high, variable temperatures is lost slowly upon transfer to benign conditions. *The Journal of Experimental Biology* **223**, 13.

Ni, Z.-P., Wu, L.-G. & Zhang, L. 2013 Analysis on forecasting errors and associated circulations of sudden typhoon track changes during 2005–2010. *Meteorological Monthly* **39** (6), 719–727.

Nie, J. J., Fan, J. H., Yang, R. S. & Yang, J.-H. 2014 Some statistical correlation analyses for Fermi/Lat blazars. *Science China Physics, Mechanics & Astronomy* **57** (10), 2007–2025.

Pan, Y.-F. & Wu, M. 2012 Analysis on the necessity and practice of shellfish aquaculture insurance. *Shanghai Insurance* **7**, 45–46.

Pan, C., Li, J., Xu, T. & Wang, G. 2017 Operational analysis of meteorological index insurance in the farming of South American white shrimp. *China Insurance* **02**, 47–50.

Patricola, C., Cassidy, D. J. & Klotzbach, P. 2022 Tropical oceanic influences on observed global tropical cyclone frequency. *Geophysical Research Letters* **49**, 1–10. doi:10.1029/2022GL099354.

Qin, L.-J., Dong, Q. & Xue, C.-J. 2015 Seasonal to decadal variations of tropical cyclone genesis in Northwestern Pacific in recent three decades. *Marine Environmental Science* **34** (5), 723–728.

Ramsay, H. A., Camargo, S. J. & Kim, D. 2011 Cluster analysis of tropical cyclone tracks in the southern hemisphere. *Climate Dynamics* **39**, 897–917. doi:10.1007/s00382-011-1225-8.

Roberts, E., Newcomb, L., McCartha, M., Harrington, K., LaFramboise, S., Carrington, E. & Sebens, K. 2021 Resource allocation to a structural biomaterial: Induced production of byssal threads decreases growth of a marine mussel. *Functional Ecology* **35**, 1222–1239.

Seuront, L., Nicastro, K. R., Zardi, G. I. & Goberville, E. 2019 Decreased thermal tolerance under recurrent heat stress conditions explains summer mass mortality of the blue mussel *Mytilus edulis*. *Scientific Reports* **9**, 17498.

Sha, W., Shi, S.-H. & Shen, Q.-F. 2003 Effects of typhoon Rammasun on waves and marine engineering in Changjiang Estuary. *Marine Forecasts* **20** (2), 24–29.

Skok, G., Bacmeister, J. T. & Tribbia, J. 2013 Analysis of tropical cyclone precipitation using an object-based algorithm. *Journal of Climate* **26**, 2563–2579.

Tang, D.-L. & Sui, G.-J. 2015 *Typhoon Disaster Assessment and Emergency Management*. Science Press, Beijing, China.

Tu, J.-Y., Chen, J.-M., Wu, L. & Chi, C.-Z. 2019 Inter-decadal and inter-annual variability of meridional tropical cyclone activity during September–October in the northwestern North Pacific after 1998. *International Journal of Climatology* **40** (3), 1686–1702.

Wang, J. 2014 Research on meteorological index-based aquaculture insurance. *Insurance Research* **03**, 63–69.

Wang, R. & Zheng, X. 2004 Progress of marine shellfishes culture in China and its prospect. *Periodical of Ocean University of China* **34** (5), 775–780.

Wang, L., Xu, Y.-T., Xu, Z.-Y. & Chen, M.-T. 2018 Study on the cause of the sudden change in the path and strength of typhoon 'Haikui'. *Marine Forecasts* **35** (5), 93–103.

Wu, N.-G., Lin, L.-X., Li, T.-R., Huang, Z. & Chen, L.-S. 2007 Diagnosis of northward-deflecting track of typhoon Prapiroon caused by the environmental flow field and typhoon structure variation. *Meteorological Monthly* **33** (11), 9–15.

Wu, Z.-L., Chen, L.-R., Wang, K., Zhang, S.-Y. & Bi, Y.-X. 2020 Morphological characteristics of vesicle of *Sargassum horneri* and its relationship to environmental factors in Gouqi Island. *Journal of Fisheries of China* **44** (5), 793–804.

Wu, Z., Huang, L., Wang, F., Zhang, S.-M. & Zhang, S.-Y. 2021 Impacts of tropical cyclones on mussel culture area and yield in Shengsi. *Journal of Agricultural Science and Technology* **23** (06), 171–183.

Xi, G. & Xu, W. 2006 *China Meteorological Disaster Ceremony-Zhejiang Volume*. Meteorological Press, Beijing, China.

Xiao, F., Yin, Y., Luo, Y., Song, L.-C. & Ye, D.-X. 2011 Tropical cyclone hazards analysis based on tropical cyclone potential impact index. *Journal of Geographical Sciences* **21**, 791–800. doi:10.1007/s11442-011-0880-3.

Yan, Y.-F., Tan, J.-G., Cui, L.-L., Yue, C.-J., Guo, W. & Liu, D.-W. 2019 Estimating the short-time severe precipitation of typhoon Meranti and its evolution by using the infrared brightness temperature data from Himawari-8 satellite with high spatio-temporal resolution. *Meteorological Monthly* **45** (3), 318–329.

Ying, M., Zhang, W., Yu, H., Lu, X.-Q., Feng, J.-X., Fan, Y.-X., Zhu, Y.-T. & Chen, D.-Q. 2014 An overview of the China Meteorological Administration tropical cyclone database. *Journal of Atmospheric and Oceanic Technology* **31** (2), 287–301.

Yu, J., Tang, D. L., Chen, G. B., Li, Y.-Z., Huang, Z.-R. & Wang, S.-F. 2014 The positive effects of typhoons on the fish CPUE in the South China Sea. *Continental Shelf Research* **84**, 1–12.

Yue, S., Ouarda, T. B. M. J., Bobée, B., Legendre, P. & Bruneau, P. 1999 The Gumbel mixed model for flood frequency analysis. *Journal of Hydrology* **228**, 3–4, 283.

Zhang, Z.-X., Yu, F., Guo, J.-S., Ge, R.-F., Guo, B.-H. & Xu, Y. 2006 Some problems with the plotting of objective analysis map of marine environmental elements. *Advances in Marine Science* **24** (3), 371–378.

Zhang, S., Mi, W., Wu, Z., Fan, W., Liu, H.-B., Fang, Z.-Q. & Zhu, W.-B. 2017 Discussion on the application of meteorological index insurance in aquaculture. *Fishery Information & Strategy* **32** (3), 180–184.

Zhou, D.-C. & Duan, Z.-D. 2003 The Gumbel-logistic model for joint probability distribution of extreme-value wind speeds and effective wave heights. *The Ocean Engineering* **21** (2), 45–51.

Zhou, H., Guo, S.-H. & Feng, Z.-G. 2014 *Zhejiang Islands*. Ocean Press, Beijing, China.

Zhoushan Bureau of Statistics. 2018 *Statistical Yearbook of Zhoushan*. China Statistics Press, Beijing, China.

Zhoushan Statistics Bureau. 2021 Statistical Yearbook of Zhoushan. http://zstj.zhoushan.gov.cn/col/index.html. 2022-01-07.

First received 3 August 2023; accepted in revised form 1 January 2024. Available online 23 January 2024